electronic materials

MDPI

Article

Structural, Electronic, and Optical Properties of *p*-Type Semiconductors Cu_2O and $ZnRh_2O_4$: A *Self-Consistent* Hybrid Functional Investigation

Daniel Fritsch

Department Structure and Dynamics of Energy Materials, Helmholtz-Zentrum Berlin für Materialien und Energie, Hahn-Meitner-Platz 1, 14109 Berlin, Germany; daniel.fritsch@helmholtz-berlin.de

Abstract: The *p*-type semiconductors Cu_2O and $ZnRh_2O_4$ have been under investigation for potential applications as transparent conducting oxides. Here, we re-evaluate their structural, electronic, and optical properties by means of *first-principles* calculations employing density functional theory and a recently introduced *self-consistent* hybrid functional approach. Therein, the predefined fraction α of Hartree–Fock exact exchange is determined self-consistently via the inverse of the dielectric constant ε_∞. The structural, electronic, and optical properties will be discussed alongside experimental results, with a focus on possible technological applications.

Keywords: Cu_2O; $ZnRh_2O_4$; semiconductor; transparent conducting oxide; density functional theory; hybrid functional; band structure; dielectric function

check for updates

Citation: Fritsch, D. Structural, Electronic, and Optical Properties of *p*-Type Semiconductors Cu_2O and $ZnRh_2O_4$: A *Self-Consistent* Hybrid Functional Investigation. *Electron. Mater.* **2021**, *2*, 504–510. https://doi.org/10.3390/electronicmat2040035

Academic Editor: Dong Jiang

Received: 31 July 2021
Accepted: 18 October 2021
Published: 1 November 2021

Publisher's Note: MDPI stays neutral with regard to jurisdictional claims in published maps and institutional affiliations.

Copyright: © 2021 by the author. Licensee MDPI, Basel, Switzerland. This article is an open access article distributed under the terms and conditions of the Creative Commons Attribution (CC BY) license (https://creativecommons.org/licenses/by/4.0/).

1. Introduction

Transparent conducting oxides (TCOs) are one important building block of current technological devices, ranging from various display applications to solar cells. While the quest to find new and environmentally friendly TCOs has resulted in the identification of numerous *n*-type TCOs, their *p*-type counterparts are much harder to come by. This apparent scarcity of *p*-type TCOs suitable for device applications has led to a surge in experimental and theoretical investigations, trying to understand the underlying reasons and formulating some design principles for specific necessary material properties [1].

The present work focuses on two identified examples for *p*-type TCOs, namely cuprous oxide (Cu_2O) and $ZnRh_2O_4$. Cu_2O crystallises in the cubic crystal structure (space group $Pn\bar{3}m$, no. 224), whereas $ZnRh_2O_4$ crystallises in the so-called *normal* spinel crystal structure (space group $Fd\bar{3}m$, no. 227), respectively, similar to $ZnFe_2O_4$ [2], but at variance to $NiFe_2O_4$ and $CoFe_2O_4$ which crystallise in the (partially) *inverse* spinel structure [3]. In general, the spinel crystal structure offers a rich interplay of structural parameters [4], subsequently influencing the electronic and optical properties of materials and allowing for a plethora of potential technological applications [5].

While Cu_2O has been known as a *p*-type semiconductor for decades, the spinel-type $ZnRh_2O_4$ received wider attention only fairly recently [6,7]. Subsequent *first-principles* calculations of the whole spinel series ZnM_2O_4 (M = Co, Rh, and Ir) tried to identify their conduction mechanism, i.e., hole or polaron conduction [8–10]. These *first-principles* calculations employed a range of (semi)local and hybrid exchange and correlation functionals to investigate the structural, electronic, and optical properties of $ZnRh_2O_4$, respectively. Application of exchange and correlation functionals of increased complexity has been recognised as a viable tool for a better description of material properties [11].

The recent development of a *self-consistent* hybrid functional [12] provided the motivation for the current work, namely to re-evaluate the structural, electronic, and optical properties of Cu_2O and $ZnRh_2O_4$, similar to other crystalline [13,14] and amorphous [15,16] oxide TCOs.

The paper is organised as follows. Section 2 shortly introduces the *self-consistent* hybrid functional approach and provides the necessary computational details. In Section 3 the results on the structural (Section 3.1), and electronic and optical (Section 3.2) properties are presented and discussed alongside experimental data and other theoretical investigations. Section 4 provides a short summary and outlook.

2. Theoretical Background

The *first-principles* calculations presented here employed both, the state-of-the-art meta-GGA SCAN functional [17] and a recently introduced *self-consistent* hybrid functional (scPBE0) [12,13]. While the SCAN functional fulfils all the necessary requirements of an exchange and correlation functional, it has been claimed that its accuracy in terms of predicting structural properties rivals that of computationally much more demanding hybrid exchange and correlation functionals [18]. On the other hand, the so-called hybrid exchange and correlation functionals admix a predefined fraction α of Hartree–Fock exact exchange into the underlying (semi)local functional and allow for a much improved description of electronic and optical properties of materials. Here, the recently introduced *self-consistent* hybrid functional has been employed, where the particular fraction of Hartree–Fock exact exchange α is treated as a material specific parameter, determined via an additional self-consistency cycle and employing the reciprocal relationship between α and the low-frequency dielectric constant ε_∞, i.e., $\alpha = 1/\varepsilon_\infty$. The dielectric constant is calculated for the identified ground state structure for each iteration, until their difference between successive iterations is smaller than 0.01 [13,14].

All the calculations of the present work have been performed using the Vienna *Ab Initio* Simulation Package (VASP 5.4.4) [19–21] together with the projector-augmented wave (PAW) formalism [22,23]. Standard PAW potentials supplied by VASP have been employed, contributing 11, 12, 15, and 6 valence electrons for the Cu, Zn, Rh, and O atoms, respectively.

Ground state structural properties have been obtained from analysing the total energy curves, i.e., monitoring changes in the total energy with respect to several fixed volumes around the ground state volume, followed by a subsequent analysis via Murnaghan's equation of state [24,25], yielding ground state volumes and lattice parameters, and giving additional access to the bulk modulus B_0 and its pressure derivative B_0', respectively. From previous investigations on spinel ferrites it is known that both, lattice parameters and bulk modulus, have to agree with the experimental values in order to identify the correct ground state structure [26].

Based on the ground state structural properties the electronic (band structures) and optical properties (dielectric functions) have been calculated. For the latter, the number of empty bands in the calculations have been increased by a factor of three, in order to allow for a sufficient capture of the influence of higher lying energy bands on the optical properties.

Other calculational parameters include a 500 eV cutoff for the plane wave expansion, convergence criteria of 10^{-6} eV and 10^{-3} Å^{-1} for the calculated total energies and forces on the atoms, respectively, and a $6 \times 6 \times 6$ Γ-centred k-point grid, respectively, thus ensuring well-converged results for the structural, electronic, and optical properties.

3. Results and Discussion

3.1. Structural Properties

Figure 1 shows the total energy curves (upper panels) for Cu_2O (left panel) and $ZnRh_2O_4$ (right panel), calculated with the SCAN (black), PBE0 (red), and scPBE0 (green) exchange and correlation functionals. The dashed lines indicate their respective ground state values, while the orange dashed line refers to the experimental results. Subsequent analysis of the total energy curves yields the ground state volumes and lattice parameters, the bulk modulus B_0 and its pressure derivative B_0', respectively, summarised and compared to available experimental results in Table 1.

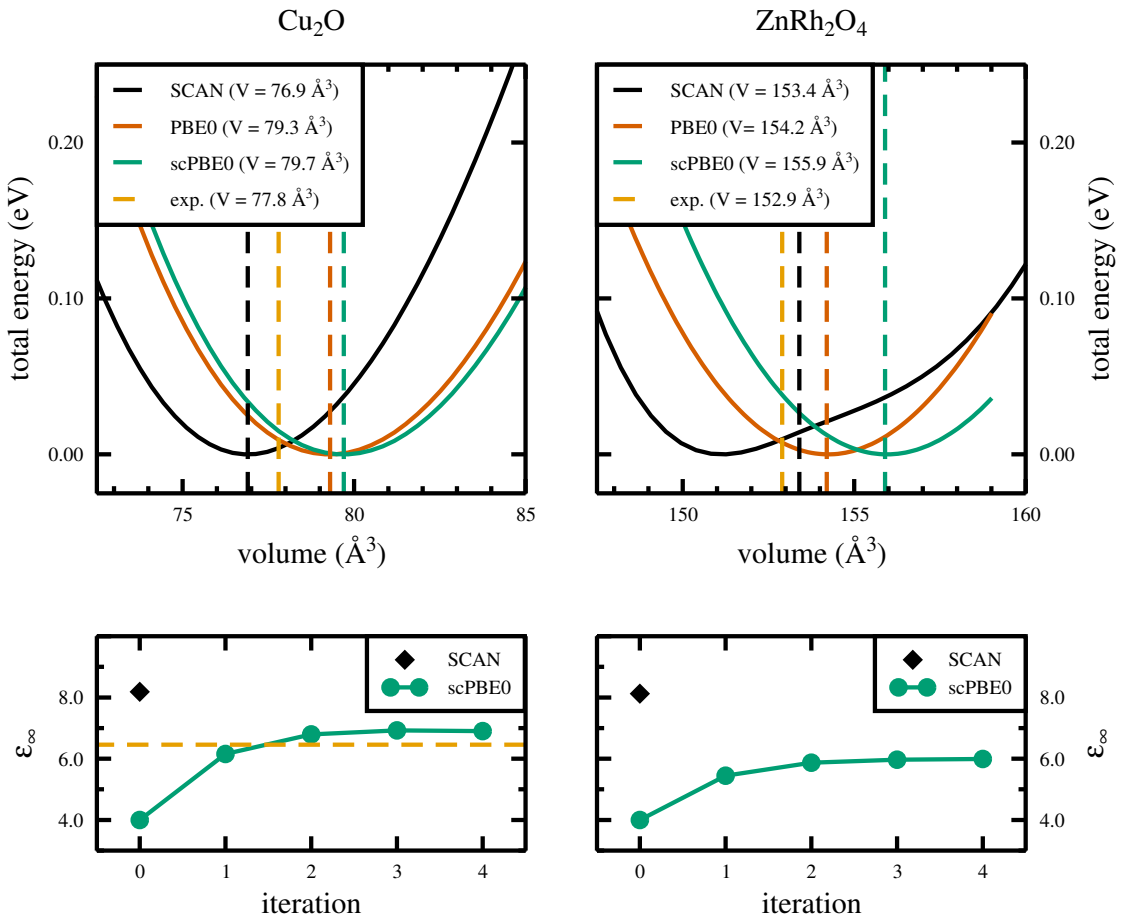

Figure 1. Upper panels: total energy (in eV) with respect to the unit cell volume for Cu_2O (**left panel**) and $ZnRh_2O_4$ (**right panel**) calculated by means of the SCAN (black) PBE0 (red), and scPBE0 (green) exchange and correlation functionals, respectively. The dashed orange lines refer to the experimental data summarised in Table 1. **Lower panels**: convergence for the dielectric constant ε_∞ is obtained after four steps in the additional self-consistency cycle of the scPBE0 exchange and correlation functional. For comparison, the black diamonds and dashed orange line depict the SCAN calculated ε_∞ and experimental data summarised in Table 1.

Table 1. Ground state structural properties for Cu_2O and $ZnRh_2O_4$ for different exchange and correlation functionals in comparison to experimental data. Shown are the lattice constants a [Å], the internal anion displacement parameter u (for $ZnRh_2O_4$), the bulk modulus B_0 [GPa] and its pressure derivative B_0', the calculated dielectric constant ε_∞ and the corresponding α value, and the Kohn–Sham energy band gap E_{KS} [eV], respectively.

Cu_2O	**SCAN**	**PBE0**	**scPBE0**	**Exp.**
a [Å]	4.252	4.296	4.303	4.2685 [27], 4.2696 [28]
B_0 [GPa]	122.0	110.8	109.8	110.6 [29], 111.96 [30]
B_0'	4.9	4.6	4.6	4.46 [30]
ε_∞	8.186	6.153	6.922	6.46 [28]
α	0.122	0.250	0.147	0.15 [28]
E_{KS} [eV]	0.559	2.685	1.703	2.1720 [31]
$ZnRh_2O_4$	**SCAN**	**PBE0**	**scPBE0**	**Exp.**
a [Å]	8.498	8.513	8.544	8.489 [32]
u	0.260	0.261	0.261	–
B_0 [GPa]	196.9	205.4	198.3	–
B_0'	6.9	3.6	3.6	–
ε_∞	8.125	5.445	5.990	–
α	0.123	0.250	0.168	–
E_{KS} [eV]	0.989	3.666	2.707	2.1 [33], 2.74 [32]

For Cu_2O the lattice constants amount to 4.252 Å, 4.296 Å, and 4.303 Å for the SCAN, PBE0, and scPBE0 exchange and correlation functionals, in good agreement with the experimental lattice constants 4.2685 Å [27] and 4.2696 Å [28]. While the SCAN lattice constant is underestimated with respect to the experimental values, the PBE0 value is similarly good, and the scPBE0 value is slightly overestimated. The bulk moduli B_0 amount to 122.0 GPa, 110.8 GPa, and 109.8 GPa, again for the SCAN, PBE0, and scPBE0 exchange and correlation functionals. While the SCAN value is overestimated with respect to the experimental values of 110.6 GPa [29] and 111.96 GPa [30], PBE0 and scPBE0 values show similarly good agreement. The same holds for the pressure derivative B_0' of the bulk modulus, with PBE0 and scPBE0 values of 4.6 showing best agreement with the experimental value of 4.46 [30].

The ground state crystal structures served as a starting point for subsequent calculations of the dielectric constant ε_∞, amounting to 8.186 for the SCAN exchange and correlation functional, overestimated with respect to the experimental value of 6.46 [28], respectively. Much better agreement is obtained for the PBE0 exchange and correlation functional with ε_∞ amounting to 6.153, iterated to self-consistency within four steps for the scPBE0 exchange and correlation functional, amounting to 6.922, respectively, again in good agreement with the experimental value. The convergence of ε_∞ for Cu_2O within the scPBE0 approach is shown in the lower left panel of Figure 1.

The lattice constants of $ZnRh_2O_4$ amount to 8.498 Å, 8.513 Å, and 8.544 Å, again calculated by means of the SCAN, PBE0, and scPBE0 exchange and correlation functionals. This is in favourable agreement with the experimental lattice constant of 8.489 Å [32]. Interestingly, the SCAN value shows the best agreement, and the scPBE0 value is again larger than the PBE0 one. The internal oxygen parameter u, the bulk modulus B_0 and its pressure derivative B_0' are all in agreement with other theoretical investigations employing various types of exchange and correlation functionals.

Again, the ground state crystal structures served as starting points for calculating the dielectric constant ε_∞, yielding a large 8.125 for the SCAN exchange and correlation functional. Similar to Cu_2O, self-consistency in the calculation of ε_∞ is reached after four steps, starting from 5.445 (PBE0) to 5.990 (scPBE0), respectively.

3.2. Electronic and Optical Properties

The determined ground state structural properties allowed for subsequent analysis of the electronic and optical properties. The calculated electronic band structures are shown in the upper panels of Figure 2 for Cu_2O (left) and $ZnRh_2O_4$ (right), respectively.

Shown are the valence (green) and conduction bands (red), calculated by means of the *self-consistent* hybrid functional scPBE0, with the valence band maximum set to zero. The shaded grey area depicts the calculations employing the SCAN exchange and correlation functional.

For Cu_2O the band gap is direct and at the Γ point, amounting to 0.559 eV, 2.685 eV, and 1.703 eV for calculations employing the SCAN, PBE0, and scPBE0 exchange and correlation functionals. The best agreement with the experimental result of 2.1720 eV [31] is observed for the hybrid functionals PBE0 and scPBE0. Interestingly, iterating the fraction α of Hartree–Fock exact exchange to self-consistency reduces the band gap considerably and yields better agreement with the experiment.

For $ZnRh_2O_4$ the band gap is indirect with the valence band maximum at X and the conduction band minimum closely to X along the X—Γ line. The band gaps amount to 0.989 eV, 3.666 eV, and 2.707 eV for calculations employing the SCAN, PBE0, and scPBE0 exchange and correlation functionals. Again, the best agreement with the experimental band gap of 2.74 eV [32] is observed for the scPBE0 exchange and correlation functional.

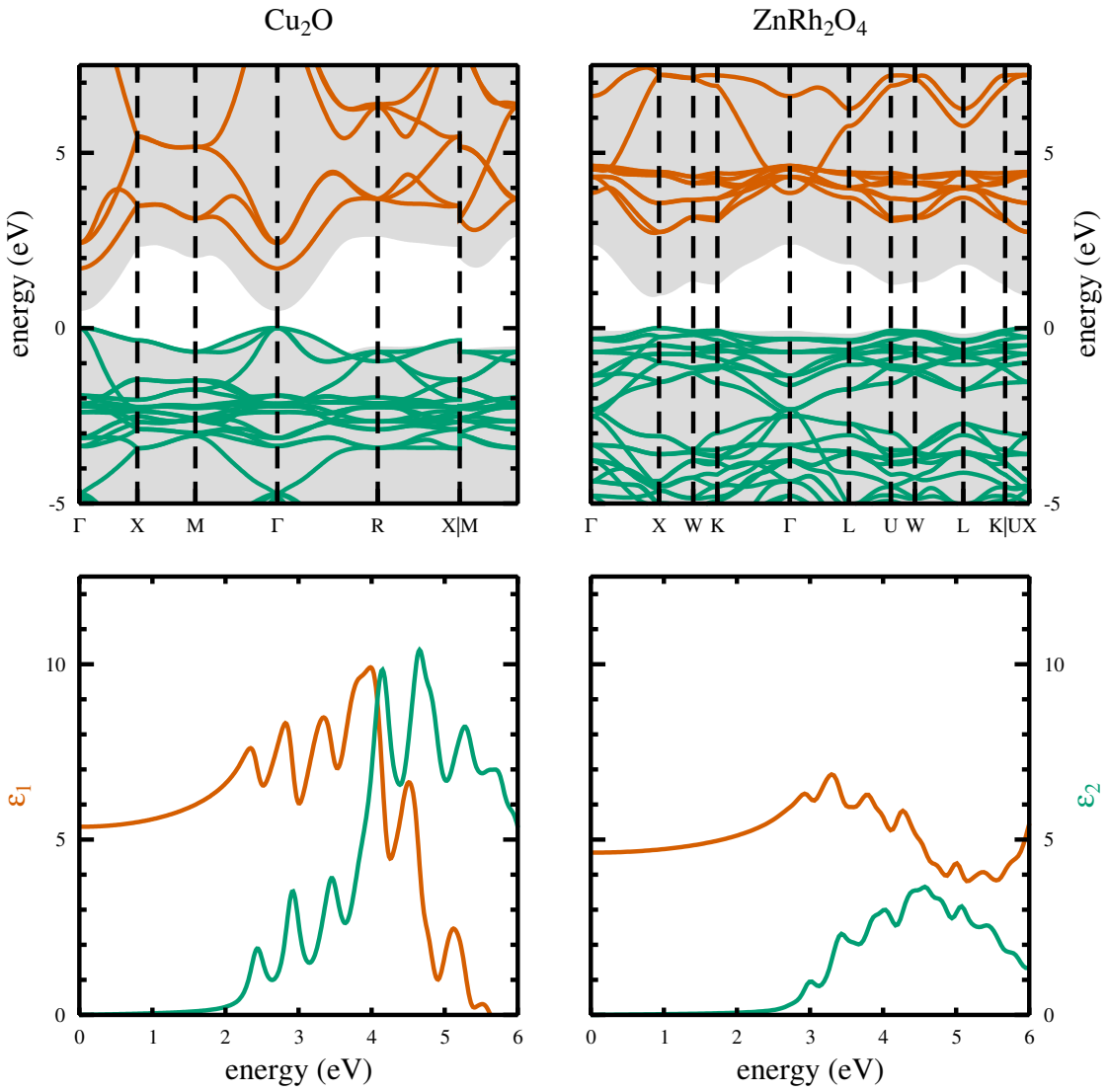

Figure 2. Upper panels: electronic band structures for Cu_2O **(left panel)** and $ZnRh_2O_4$ (**right panel**) calculated by means of the *self-consistent* hybrid exchange and correlation functional scPBE0. Shown are the valence (green) and conduction bands (red), whereas the shaded grey backgrounds indicate the results for the SCAN exchange and correlation functional. Energies are in electron volt (eV) and the valence band maximum is set to zero. **Lower panels**: optical properties for Cu_2O (**left panel**) and $ZnRh_2O_4$ (**right panel**). Shown are the ε_1 real (red) and ε_2 imaginary (green) parts of the dielectric functions, calculated by means of the scPBE0 exchange and correlation functional.

This is consistent with earlier hybrid functional calculations yielding 2.87 eV [9]. Scanlon et al. [9] and Wahila et al. [34] also noted that the crystal field splittings play a crucial role for the band edges in the spinel materials ZnM_2O_4 (M = Co, Rh, and Ir), and are difficult to treat with previously employed exchange and correlation functionals. As a possible solution, they suggested adjusting the fraction α of Hartree–Fock exact exchange in hybrid functional calculations. This serves as a further justification for the present work. Subsequently, a detailed *self-consistent* hybrid functional investigation for spinel materials ZnM_2O_4 (M = Co, Rh, and Ir) is underway, and will be published elsewhere.

Following the calculation of the band structures, the optical properties have been calculated as well. The obtained ε_1 real (red) and ε_2 imaginary (green) parts of the dielectric functions are shown in the lower panels of Figure 2 for Cu_2O (left) and $ZnRh_2O_4$ (right), respectively. These calculations have been performed employing the scPBE0 exchange and correlation functional, and give additional access to absorption coefficients and reflectivity for better comparison with experimental data.

4. Summary and Outlook

Here, a detailed *first-principles* investigation re-evaluated the structural, electronic, and optical properties of two *p*-type semiconductors, namely Cu_2O and $ZnRh_2O_4$, by means of the *self-consistent* hybrid functional scPBE0. While the ground state structural properties have been better described with the standard PBE0 exchange and correlation functional, the electronic and optical properties calculated by means of the scPBE0 exchange and correlation functional are in best agreement with available experimental results. For $ZnRh_2O_4$ in particular, the question of calculating the ligand field splitting reliably by *first-principles* methods has been raised earlier. In order to address this question, investigations for the spinel materials ZnM_2O_4 (M = Co, Rh, and Ir) are underway and will be published elsewhere.

Funding: This research received no external funding.

Institutional Review Board Statement: Not applicable.

Informed Consent Statement: Not applicable.

Data Availability Statement: The data that support the findings of this study are available from the corresponding author upon reasonable request.

Acknowledgments: This work made use of computational resources provided by the North-German Supercomputing Alliance (HLRN, www.hlrn.de), and the ZEDAT and DIRAC high-performance computing facilities of the Freie Universität Berlin and the Helmholtz-Zentrum Berlin, respectively.

Conflicts of Interest: The author declares no conflict of interest.

Abbreviations

The following abbreviations are used in this manuscript:

DFT	Density functional theory
GGA	Generalised gradient approximation
TCO	Transparent conducting oxide

References

1. Hosono, H. Recent progress in transparent oxide semiconductors: Materials and device application. *Thin Solid Films* **2007**, *515*, 6000. [CrossRef]
2. Fritsch, D. Electronic and optical properties of spinel zinc ferrite: *ab initio* hybrid functional calculations. *J. Phys. Condens. Matter* **2018**, *30*, 095502. [CrossRef] [PubMed]
3. Fritsch, D.; Ederer, C. Epitaxial strain effects in the spinel ferrites $CoFe_2O_4$ and $NiFe_2O_4$ from first principles. *Phys. Rev. B* **2010**, *82*, 104117. [CrossRef]
4. Fritsch, D.; Ederer, C. Effect of epitaxial strain on the cation distribution in spinel ferrites $CoFe_2O_4$ and $NiFe_2O_4$: A density functional theory study. *Appl. Phys. Lett.* **2011**, *99*, 081916. [CrossRef]
5. Caffrey, N.; Fritsch, D.; Archer, T.; Sanvito, S.; Ederer, C. Spin-filtering efficiency of ferrimagnetic spinels $CoFe_2O_4$ and $NiFe_2O_4$. *Phys. Rev. B* **2013**, *87*, 024419. [CrossRef]
6. Kamiya, T.; Narushima, S.; Mizoguchi, H.; Shimizu, K.; Ueda, K.; Ohta, H.; Hirano, M.; Hosono, H. Electrical properties and structure of *p*-type amorphous oxide semiconductor xZnO·Rh_2O_3. *Adv. Funct. Mater.* **2005**, *15*, 968. [CrossRef]
7. Narushima, S.; Mizoguchi, H.; Shimizu, K.; Ueda, K.; Ohta, H.; Hirano, M.; Kamiya, T.; Hosono, H. A *p*-type amorphous oxide semiconductor and room temperature fabrication of amorphous oxide *p*-*n* heterojunction diodes. *Adv. Mater.* **2003**, *15*, 1409. [CrossRef]
8. Nagaraja, A.R.; Perry, N.H.; Mason, T.O.; Tang, Y.; Grayson, M.; Paudel, T.R.; Lany, S.; Zunger, A. Band or polaron: The hole conduction mechanism in the *p*-type spinel Rh_2ZnO_4. *J. Am. Ceram. Soc.* **2011**, *95*, 269. [CrossRef]
9. Scanlon, D.O.; Watson, G.W. Band gap anomalies of the $ZnM^{III}_2O_4$ (M^{III} = Co, Rh, Ir) spinels. *Phys. Chem. Chem. Phys.* **2011**, *13*, 9667. [CrossRef] [PubMed]
10. Amini, M.N.; Dixit, H.; Saniz, R.; Lamoena, D.; Partoens, B. The origin of *p*-type conductivity in ZnM_2O_4 (M = Co, Rh, Ir) spinels. *Phys. Chem. Chem. Phys.* **2013**, *16*, 2588. [CrossRef] [PubMed]
11. Fritsch, D.; Schorr, S. Climbing Jacob's ladder: A density functional theory case study for $Ag_2ZnSnSe_4$ and $Cu_2ZnSnSe_4$. *J. Phys. Energy* **2021**, *3*, 015002. [CrossRef]
12. Skone, J.H.; Govoni, M.; Galli, G. Self-consistent hybrid functional for condensed systems. *Phys. Rev. B* **2014**, *89*, 195112. [CrossRef]

13. Fritsch, D.; Morgan, B.J.; Walsh, A. Self-consistent hybrid functional calculations: Implications for structural, electronic, and optical properties of oxide semiconductors. *Nanoscale Res. Lett.* **2017**, *12*, 19. [CrossRef]
14. Fritsch, D. Self-consistent Hybrid Functionals: What We have Learned So Far. In *Theory and Simulation in Physics for Materials Applications: Cutting-Edge Techniques in Theoretical and Computational Materials Science*; Levchenko, E.V., Dappe, Y.L., Ori, G., Eds.; Springer International Publishing: Cham, The Netherlands, 2020; p. 79.
15. Fritsch, D. Amorphous Sn-Ti oxides: A combined molecular dynamics and density functional theory study. *Phys. Status Solidi A* **2018**, *215*, 1800071. [CrossRef]
16. Wahila, M.J.; Lebens-Higgins, Z.W.; Butler, K.T.; Fritsch, D.; Treharne, R.E.; Palgrave, R.G.; Woicik, J.C.; Morgan, B.J.; Walsh, A.; Piper, L.F.J. Accelerated optimization of transparent, amorphous zinc-tin-oxide thin films for optoelectronic applications. *APL Mater.* **2019**, *7*, 022509. [CrossRef]
17. Sun, J.; Ruzsinszky, A.; Perdew, J. Strongly constrained and appropriately normed semilocal density functional. *Phys. Rev. Lett.* **2015**, *115*, 036402. [CrossRef] [PubMed]
18. Sun, J.; Remsing, R.C.; Zhang, Y.; Sun, Z.; Ruzsinszky, A.; Peng, H.; Yang, Z.; Paul, A.; Waghmare, U.; Wu, X.; et al. Accurate first-principles structures and energies of diversely bonded systems from an efficient density functional. *Nat. Chem.* **2016**, *8*, 831. [CrossRef] [PubMed]
19. Kresse, G.; Hafner, J. Ab initio molecular dynamics for liquid metals. *Phys. Rev. B* **1993**, *47*, 558. [CrossRef]
20. Kresse, G.; Hafner, J. Ab initio molecular-dynamics simulation of the liquid-metal − amorphous-semiconductor transition in germanium. *Phys. Rev. B* **1994**, *49*, 14251. [CrossRef] [PubMed]
21. Kresse, G.; Furthmüller, J. Efficiency of ab initio total energy calculations for metals and semiconductors using a plane-wave basis set. *Comp. Mater. Sci.* **1996**, *6*, 15. [CrossRef]
22. Blöchl, P.E. Projector augmented-wave method. *Phys. Rev. B* **1994**, *50*, 17953. [CrossRef]
23. Kresse, G.; Joubert, D. From ultrasoft pseudopotentials to the projector augmented-wave method. *Phys. Rev. B* **1999**, *59*, 1758. [CrossRef]
24. Murnaghan, F.D. Finite deformations of elastic solids. *Am. J. Math.* **1937**, *59*, 235. [CrossRef]
25. Murnaghan, F.D. The compressibility of media under extreme pressure. *Proc. Natl. Acad. Sci. USA* **1944**, *30*, 244. [CrossRef] [PubMed]
26. Fritsch, D.; Ederer, C. Strain effects in spinel ferrite thin films from first principles calculations. *J. Phys. Conf. Ser.* **2011**, *292*, 012014. [CrossRef]
27. Kirfel, A.; Eichhorn, K. Accurate structure analysis with synchrotron radiation. The electron density in Al_2O_3 and Cu_2O. *Acta Cryst. A* **1990**, *46*, 271. [CrossRef]
28. Meyer, B.K.; Polity, A.; Reppin, D.; Becker, M.; Hering, P.; Kramm, B.; Klar, P.J.; Sander, T.; Reindl, C.; Heiliger, C.; et al. The physics of copper oxide (Cu_2O). In *Oxide Semiconductors*, *Semiconductors and Semimetals*; Svensson, B.G., Pearton, S.J., Jagadish, C., Eds.; Elsevier: Amsterdam, The Netherlands, 2013; Volume 88, p. 201.
29. Hallberg, J.; Hanson, R.C. The elastic constants of cuprous oxide. *Phys. Status Solidi B* **1970**, *42*, 305. [CrossRef]
30. Manghnani, M.H.; Brower, W.S.; Parker, H.S. Anomalous elastic behavior in Cu_2O under pressure. *Phys. Status Solidi A* **1974**, *25*, 69. [CrossRef]
31. Uihlein, C.; Fröhlich, D.; Kenklies, R. Investigation of exciton fine structure in Cu_2O. *Phys. Rev. B* **1981**, *23*, 2731. [CrossRef]
32. Dekkers, M.; Rijnders, G.; Blank, D.H.A. $ZnIr_2O_4$, a *p*-type transparent oxide semiconductor in the class of spinel zinc-d^6-transition metal oxide. *Appl. Phys. Lett.* **2007**, *90*, 021903. [CrossRef]
33. Mizoguchi, H.; Hirano, M.; Fujitsu, S.; Takeuchi, T.; Ueda, K.; Hosono, H. $ZnRh_2O_4$: A *p*-type semiconducting oxide with a valence band composed of a low spin state of Rh^{3+} in a $4d^6$ configuration. *Appl. Phys. Lett.* **2002**, *80*, 1207. [CrossRef]
34. Wahila, M.J.; Lebens-Higgins, Z.W.; Jackson, A.J.; Scanlon, D.O.; Lee, T.L.; Zhang, J.; Zhang, K.H.L.; Piper, L.F.J. Band edge evolution of transparent $ZnM_2^{III}O_4$ (M^{III} = Co, Rh, Ir) spinels. *Phys. Rev. B* **2019**, *100*, 085126. [CrossRef]